Original paper

Transcoronary stem cell transfer and evolution of infarct-related artery atherosclerosis: evaluation with conventional and novel imaging techniques including Quantitative Virtual Histology (qVH)

Wladyslaw Dabrowski[1,2], Lukasz Tekieli[1,2,3], Adam Mazurek[2,3], Magdalena Lanocha[4], R. Pawel Banys[5], Krzysztof Zmudka[1,2], Marcin Majka[6], Wojciech Wojakowski[7], Michal Tendera[7], Piotr Musialek[2,3]

[1]Department of Interventional Cardiology, Jagiellonian University Institute of Cardiology, Krakow, Poland
[2]John Paul II Hospital, Krakow, Poland
[3]Department of Cardiac and Vascular Diseases, Jagiellonian University, Institute of Cardiology, John Paul II Hospital, Krakow, Poland
[4]St. Adalbert's Hospital, Poznan, Poland
[5]Department of Radiology, John Paul II Hospital, Krakow, Poland
[6]Jagiellonian University Department of Transplantation, Krakow, Poland
[7]Division of Cardiology and Structural Heart Diseases, Medical University of Silesia, Katowice, Poland

Adv Interv Cardiol 2022; 18, 4 (70): 483–495
DOI: https://doi.org/10.5114/aic.2023.125609

Abstract

Introduction: It has been suggested that infarct-related artery (IRA) atherosclerosis progression after stem cell transcoronary administration might represent a stem-cell mediated adverse effect.

Aim: To evaluate, using conventional (quantitative coronary angiography, QCA, intravascular ultrasound – IVUS) and novel (quantitative virtual histology – qVH) tools, evolution of IRA atherosclerosis following transcoronary stem cell transfer.

Material and methods: QCA, IVUS, VH-IVUS and qVH were performed in 22 consecutive patients (4 women) aged 59 years (data provided as median) undergoing a distal-to-stent infusion of 2.21×10^6 $CD34^+CXCR4^+$ autologous bone marrow cells via a cell delivery-dedicated perfusion catheter at anterior AMI day 7. Imaging was repeated at 12 months. This was a substudy of Myocardial Regeneration by Intracoronary Infusion of Selected Population of Stem Cells in Acute Myocardial Infarction (REGENT) Trial (NCT00316381).

Results: 18.2% subjects showed absence of distal-to-stent angiographic/IVUS atherosclerotic lesion(s) at baseline and no new lesion(s) at 12-months. In the remaining cohort, there were 28 lesions by QCA (32 by IVUS) at baseline and no new lesion(s) at follow-up. Three fibroatheromas evolved (2 to calcified fibroatheroma and 1 to a fibrocalcific lesion); other plaques maintained their stable (low-risk) phenotypes. Diameter stenosis of QCA-identified lesions was 29.5 vs. 26.5% ($p = 0.012$, baseline vs. 12-months). Gray-scale IVUS showed reduction in area stenosis (33.8 vs. 31.0%, $p = 0.004$) and plaque burden (66.27 vs. 64.56%, $p = 0.009$) at 12-months. Peak fibrotic plaque content increased from 70.41% to 75.0% ($p = 0.004$). qVH peak confluent necrotic core area and minimal fibrous cap thickness remained stable (0.64 vs. 0.59 mm^2, $p = 0.290$, and 0.15 vs. 0.16 mm, $p = 0.646$).

Conclusions: This study, using a range of classic and novel imaging techniques, indicates lack of any stimulatory effect of transcoronary stem cell transfer on coronary atherosclerosis. Whether, and to what extent, a moderate reduction in plaque burden and stenosis severity at 12-months results from optimized pharmacotherapy and/or stem cell transfer requires further elucidation.

Key words: stem cells, progenitor cells, transcoronary administration, atherosclerosis.

Corresponding author:
Piotr Musialek, MD DPhil, Department of Cardiac and Vascular Diseases, Jagiellonian University, John Paul II Hospital, Krakow, Poland, e-mail: pmusialek@szpitaljp2.krakow.pl
Received: 6.05.2022, **accepted:** 21.10.2022.

Summary

There are conflicting data on a potential relationship between transcoronary stem cell transfer and progression of atherosclerosis. Some, mostly small-size and poorly controlled, clinical studies hypothesized that transcoronary-administered stem cells might stimulate atherosclerosis whereas some other (mostly basic research) investigations suggest several mechanisms whereby different types of stem cells might inhibit progression of atherosclerosis. Using a range of classic and novel imaging techniques we performed a longitudinal investigation in consecutive patients receiving transcoronary stem cell administration in the sub-acute phase of myocardial infarction. We found no stimulatory effect of transcoronary stem cell transfer on coronary atherosclerosis; a finding that is reassuring for clinical studies employing the transcoronary avenue as the route of choice for delivery of stem cell-based therapies to compromised myocardium. By intravascular ultrasound there was a moderate reduction in stenosis severity at 12-months and the lesions maintained low-risk lesion phenotypes on virtual histology assessment. Whether this apparent benefit is related to pharamacologic therapy and/or stem cell transfer requires further elucidation.

Introduction

Despite unquestionable progress in pharmaco- and device therapies of atherosclerosis and consequences of atherosclerosis-elicited ischaemic events, the burden of ischaemic heart disease (including ischaemic heart failure as a result of myocardial infarction(s)) is anticipated to further increase in the next 2 decades [1, 2]. Cell-based therapies aimed to stimulate myocardial repair and regeneration play an important role in current strategic agenda for cardiovascular research [1, 3]. Presently, cardiovascular cell-based therapies are undergoing some critical refinements [4–6]. Nevertheless, safety and minimization of any potential adverse effects remain as fundamental considerations in both early clinical studies and later-stage trials [4, 7].

The transcoronary route has been the principal avenue for stem/progenitor cell delivery to the myocardium, particularly in the setting of acute myocardial infarction (AMI) [8–10], using either a conventional "stop-flow" technique [9] or, more recently, physiologic perfusion techniques of cell delivery [11–14]. Some, mostly small-size and uncontrolled, studies hypothesized that transcoronary administration of stem cells might stimulate progression of atherosclerosis [15, 16], raising a potential concern for clinical trials using transcoronary cell delivery.

Aim

We prospectively evaluated, using conventional (quantitative coronary angiography (QCA), intravascular ultrasound (IVUS) and traditional VH-IVUS) and novel (quantitative virtual histology – qVH) imaging tools, evolution of infarct-related artery (IRA) atherosclerosis following transcoronary stem cell transfer via IRA.

Material and methods

We performed an investigator-initiated substudy of the Myocardial Regeneration by Intracoronary Infusion of Selected Population of Stem Cells in Acute Myocardial Infarction (REGENT) Trial (NCT00316381) [8]; it included the REGENT patients receiving autologous $CD34^+CXCR4^+$ cells in our center. Detailed inclusion/exclusion criteria were provided previously [8]. In short, inclusion criteria were as follows: anterior (AMI), successful primary percutaneous intervention (pPCI) with stent implantation in the proximal segment of IRA (left anterior descending coronary artery – LAD) within 12 h after the symptom onset, reduced left-ventricular ejection fraction (LVEF) $\leq 40\%$, and age 18–75 years. Fundamental exclusion criteria were prior MI, presence of significant stenoses in other coronary vessels requiring revascularization, past or present malignancy, or contraindications to magnetic resonance imaging (cMRI). All patients received medications as recommended by current guidelines.

On a median day 7 post stent-assisted pPCI, infusion $CD34^+$ $CXCR4^+$ selected autologous bone marrow stem cells was performed via the artery supplying the region of the myocardium affected by the infarction (LAD). Stem cells were administered through a stemcell delivery-dedicated perfusion catheter [11], positioned immediately distal to the stent in the LAD, according to the REGENT study protocol [8]. Baseline coronary angiography and intravascular ultrasound interrogation of LAD distal to stent was performed immediately prior to administration of stem cells. Imaging was repeated at 12 months. Off-line QCA analysis of LAD distal to stent was performed consistent with a typical core laboratory protocol including determination of minimal lumen diameter, MLD, and diameter stenosis, DS). ACOM.PC software (Siemens) was used; image analysis was performed by agreement of two experienced analysts. Cross-sectional plaque images were acquired with 20-MHz phased-array piezoelectric intravascular ultrasound (IVUS, 20MHz Volcano-Philips transducers, gray-scale/VH and ChromaFlo image acquisition), consistent with general requirements and definitions in IVUS and VH-IVUS imaging [17–20]. The transducer pullback speed was 0.5 mm/s (rather than 1.0 mm/s) to minimize the risk of missing the fundamental plaque morphology spot(s) [21]. Radiofrequency backscatter data were collected simultaneously as triggered by the R-wave peak of the patient's electrocardiogram. The region of interest was defined as LAD distal to the stent(s) implanted during pPCI.

Image analysis was performed off-line. Conventional IVUS parameters, such as minimal lumen area (MLA), plaque burden (PB), and area stenosis (AS) were calculated using QIvus 2.0 software (Medis Medical Imaging Systems, the Netherlands). Corresponding images of baseline and follow-up IVUS examinations were identified by the distance from fiduciary landmarks such as side branches and stent edge. Lesion definition on IVUS required 3 consecutive frames with plaque burden > 40%.

Anonymised, matched angiogram and IVUS runs were analyzed in a random order, with the analysts blinded as to whether a particular dataset included baseline vs. follow-up data.

Besides conventional VH-IVUS measurements [22, 23], qVH analysis was performed using QIvus 2.0 software (Medis Medical Imaging Systems, the Netherlands) customized to enable measurements of several novel quantitative parameters relevant to plaque biomechanics [24, 25] (Figure 1). Matched-image analysis (including ChromaFlo images) was performed to improve the plaque luminal border determination and ensure same-site comparisons at follow-up (Figure 2). This approach overcomes one fundamental image processing limitation of conventional gray-scale and VH IVUS analysis [26]; ie., presence, on a single image, of either colorized flow definition (ChromaFlo mode) or of the VH plaque components (gray-scale and VH-IVUS mode) [21]. Conventional VH ("automatic", Figure 3) parameters (ie., the total content of necrotic core, NC; fibrofatty component, FF; fibrotic component, FT; and dense calcium, Ca) were analyzed along with the novel qVH measurements such as the minimal fibrous cap (FC) thickness, peak confluent necrotic core (cNC) parameters relevant for plaque biophysics (area, arc/angle, thickness) and other parameters (Figure 3) [21].

The "peak content" VH frame selection was performed similar to the slice selection on conventional histology by pathologists [27].

Fibroatheroma (FA) was defined as > 10% confluent necrotic core (NC) on three consecutive frames; thin cap fibroatheroma (TCFA) as FA with confluent NC on three consecutive frames and arc of NC in contact with the lumen for 36° along lumen circumference; calcified fibroatheroma (CaFA) as FA with dense calcium (Ca); fibrocalcific plaque (FiCa) as > 10% confluent Ca with no confluent NC; fibrotic plaque (FI) as < 15% fibro-fatty (FF) component and no confluent NC or Ca; pathological intimal thickening (PIT) as ≥ 600 µm thickness for > 20% of the circumference with FF > 15% and absence confluent NC or Ca [18, 20, 22, 23].

The REGENT study and IVUS substudy protocol were approved by the Institutional Ethics Committee. All subjects provided an informed written consent to participate.

Statistical analysis

Statistical analyses were performed using Statistica (version 10.0, StatSoft, Inc., Tulsa, OK, USA) or R (version 2.15.2, R Foundation, Vienna, Austria) software. Categorical data were provided as a number and (if applicable) proportion. Continuous measurements are presented as median values with lower and upper quartiles (Q1, Q3) for all variables as data distribution was mostly non-normal. IVUS imaging numeric data on IVUS examination were expressed as absolute (distance, angle, area) and relative (per cross-sectional plaque area (CSA), proportionate content) values. Differences between the two time points (B/L vs. F/U) were tested using the non-parametric Wilcoxon test. Statistical significance was defined by two-sided $p < 0.05$.

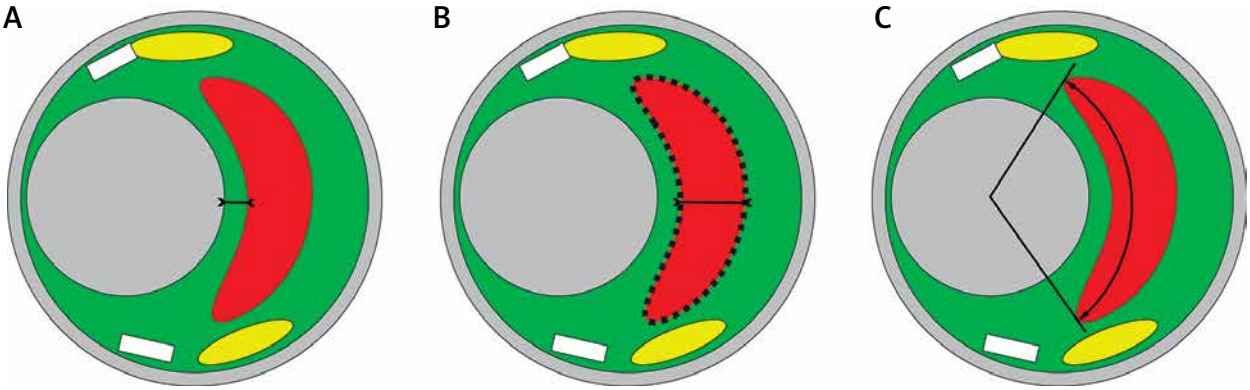

Figure 1. Schematic presentation of key components of the atherosclerotic plaque in relation to their architecture and plaque rupture risk [24, 25]. Today, these components can be quantified *in vivo* with virtual histology (VH-IVUS) using a recently validated novel VH-IVUS algorithm – quantitative virtual histology, qVH [21]. Color-coding is consistent with the VH-IVUS tissue map representation (fibrous tissue – green, necrotic core – red, calcium – white, fibro-fatty – yellow). **A** – fibrous cap thickness, **B** – necrotic core area and thickness, **C** – necrotic core angle. For a typical example of measurements performed in this study see Figure 3

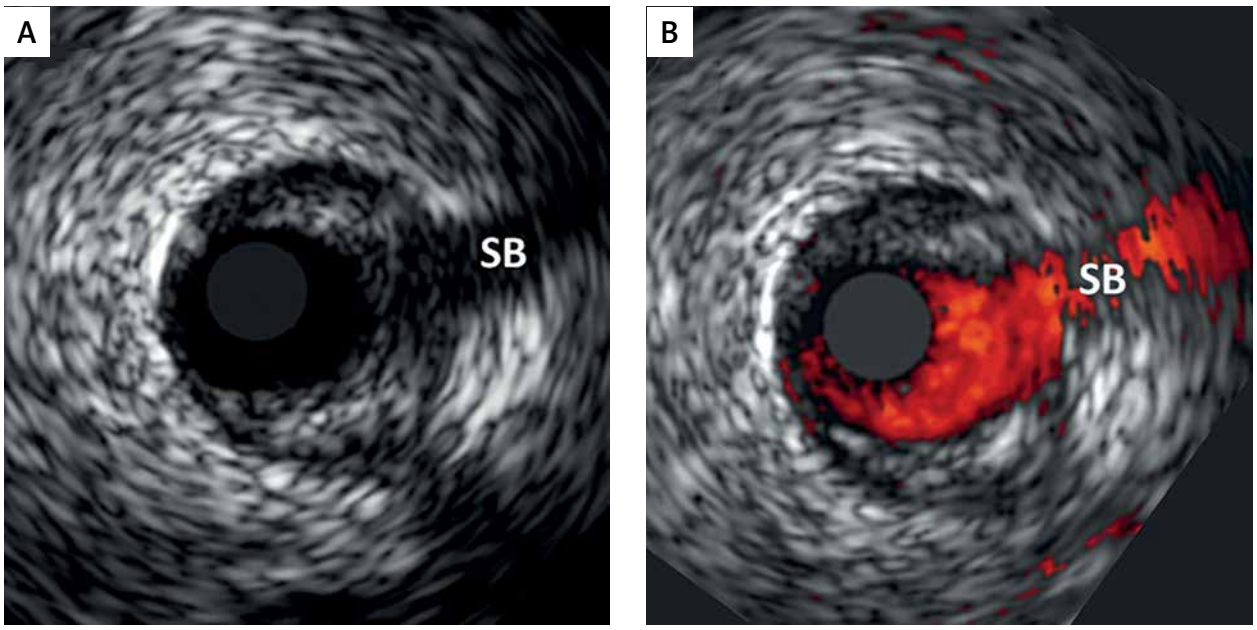

Figure 2. An illustrative example of fundamental importance of performing a matched-image (gray-scale IVUS/VH, A, and ChromaFlo, B) combined analysis to improve accuracy of the plaque luminal border delineation and ensuring same-spot analysis at baseline at follow-up. As the plaque luminal border may not be easy to determine (example in A), matched-image analysis, we introduced a routine application of a "matched image" analysis within the qVH algorithm [21]. This enables minimization of errors in plaque content quantification by VH analysis, that is critical for quantitative evaluation of the plaque composition, and in particular for the qVH measurement of fibrous cap thickness, cf. Figures 1 and 3). "Matched image" analysis plays also an important role in a longitudinal study of plaque evolution that requires a plaque image capture in the same spot (note side branch, SB, as a landmark, to minimize the likelihood of erroneous detection of a change in plaque characteristics as a result of a change in the sampling site along the arterial lumen) [28]

Results

22 consecutive patients (4 women) aged 59 (52–66) years, enrolled in our center in the REGENT Trial, formed the study group. The patients had been diagnosed with a large ST-elevation anterior wall myocardial infarction and had been treated with primary percutaneous coronary angioplasty of the proximal LAD with thrombus extraction (if feasible) [31, 32] and stent implantation. Peak CK-MB was 460 (345–767) U/l, consistent with a large myocardial tissue loss. On a (median) day 6 (baseline) left ventricular ejection fraction (LVEF) by cMRI was 38.5 (30–41)% and infarct size was 32 (22.2–40.6)%. Stent diameter was 3.0 (3.0–3.5) mm, stent(s) length was 18 (18–26) mm.

On a median day 7 post primary PCI, following a bone marrow aspiration and progenitor cell isolation, a transcoronary infusion of 2.21 (1.63–2.54) × 10^6 $CD34^+CXCR4^+$ autologous cells was performed using a transcoronary cell delivery-dedicated perfusion catheter [11].

Detailed demographic, clinical, and laboratory characteristics of the study group are presented in Table I.

At baseline, coronary imaging performed immediately prior to cell delivery showed absence of IRA atherosclerosis distal to the stent by angiography or IVUS in 18.2% patients.

In those patients no new lesions were present when imaging was repeated at 12 months. In the remaining 18 patients, there were 28 stenotic lesions by QCA whereas IVUS revealed 32 lesions. Comparison of baseline vs. 12 month follow-up QCA data showed a numeric increase in the minimal lumen diameter, from 1.43 (1.32–1.78) to 1.7 (1.36–1.94) mm but this increase did not reach statistical significance (p = 0.349). However, there was a statistically significant reduction in diameter stenosis, from 29.5 (25.5–35.5) to 26.5 (21.0–31.5)% (p = 0.012). This is consistent with not only lack of progression but, even more importantly, with angiographic regression of atherosclerosis (Table II).

Gray-scale IVUS data are provided in Table III. In brief, the minimal lumen area was 3.19 (2.46–3.92) mm^2 at baseline and 3.22 (2.59–3.94) mm^2 at 12-months (note a numeric, statistically non-significant increase, p = 0.135). However, there was a statistically significant reduction in IVUS area stenosis, from 33.75 (27.5–39.5) to 31.0 (24.15–38.0)%, p = 0.004. Similarly, IVUS plaque burden decreased from 66.27 (60.22–69.36) to 64.56 (59.93–67.85)%, p = 0.009.

Quantification of the plaque key components by VH automatic measurements of the "total" content

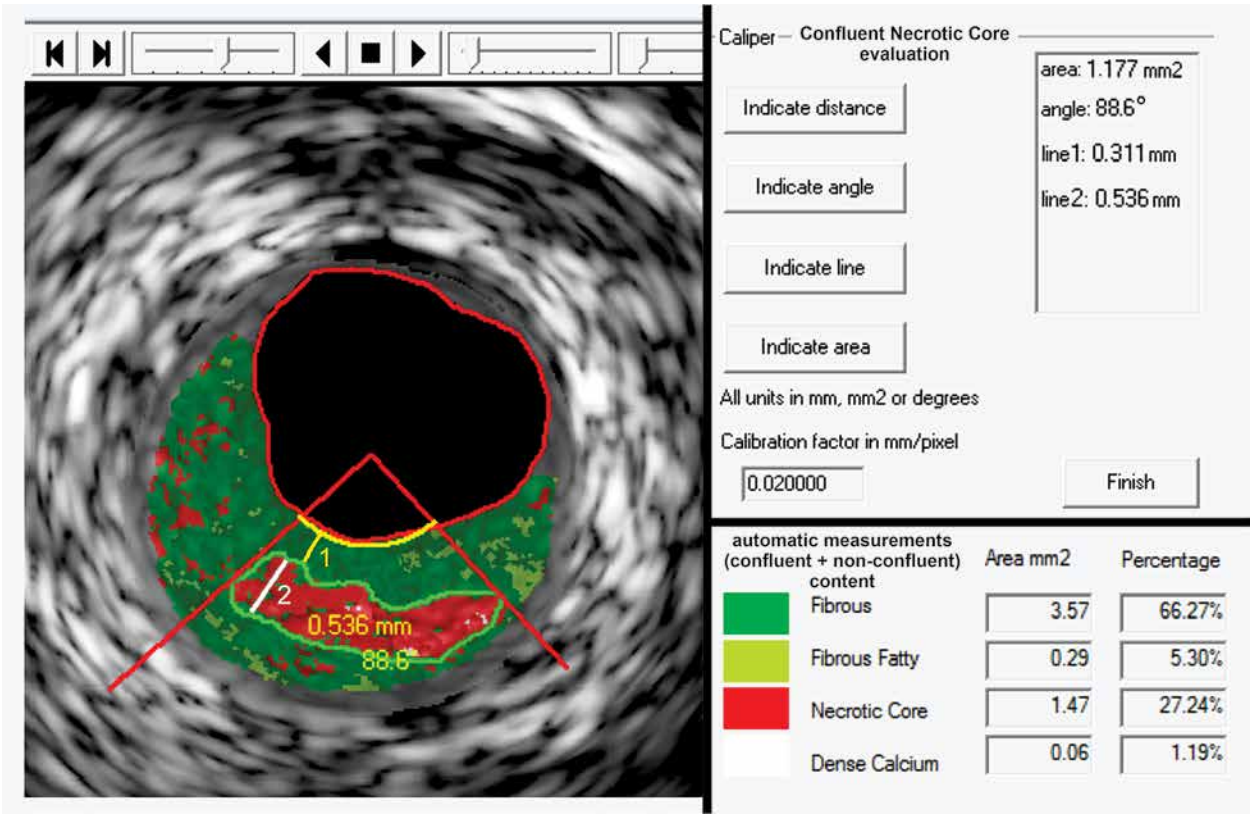

Figure 3. Typical example of quantification of key morphologic parameters of the atherosclerotic plaque using a novel image analysis algorithm (quantitative Virtual Histology, qVH). Commercially available software (QIvus 2.0, Medis Medical Imaging Systems, the Netherlands) was customized for qVH caliper and line tracking and was recently validated [21]. Confluent necrotic core is tracked on the left; numeric results of the measurements are shown in the top panel on the right. Necrotic core area – 1.177 mm^2, necrotic core angle – 88.6°, peak necrotic core thickness – 0.536 mm. This contracts with the typical "automatic" software measurements (bottom panel on the right) that consider all pixels in a given color. Note that true necrotic core area is 1.18 mm^2 rather than 1.47 mm^2. The fibrous cap minimal thickness is 0.31 mm, consistent with a thick-cap fibroatheroma. Also note that the "automatic" software quantification provides a total (per cross-sectional area) content of each of the four principal VH-IVUS–detectable plaque components (fibrous, fibro-fatty, necrotic core, dense calcium), expressed in absolute units, mm^2, or as proportion of the plaque area (%) but not of the parameters that are critical for plaque behavior in the context of rupture risk (cf., Figure 1). It may be important to realize that that the "automatic" quantification suffers from several types of artefacts, including the "calcium-associated" (pseudo) necrotic core [21, 29, 30]

per cross-sectional plaque area revealed a peak necrotic core content reduction from 0.88 (0.45–1.43) to 0.57 (0.34–1.27) mm^2 (p = 0.088) while peak fibrotic content increased from 2.5 (1.79–3.1) to 2.82 (1.93–3.66) mm^2 (p = 0.018). Total peak fibro-fatty and peak calcific content per plaque area remained stable (p = 0.978 and p = 0.559 respectively), see Figure 4.

By qVH, there was a numeric reduction in peak confluent necrotic core area from 0.64 (0.2–0.74) to 0.59 (0.31–0.73) mm^2 that, however, did not reach statistical significance (p = 0.290). The minimal fibrous cap thickness showed no change, with 0.15 (0.13–0.19) mm at baseline and 0.16 (0.13–0.2) mm at 12 months (p = 0.646). Overall, there was no progression to unstable plaque characteristics by qVH. Full data for conventional ("automatic" measurement of the "total" (fibrotic, fibro-fatty, necrotic core and dense calcium) per cross-sectional plaque area content) and qVH parameters (including other confluent necrotic core measurements and fibrous cap thickness) are provided in Table IV.

Qualitative analysis of phenotypes of the 32 plaques present at baseline showed the following: pathological intimal thickening (PIT) – 2, fibrotic (FT) – 0, fibrocalcific (FiCa) – 20, "thick"-cap fibroatheroma (FA) – 7, "thick"-cap calcified fibroatheroma (CaFA) – 3, thin-cap fibroatheroma (TCFA) – 0, calcified thin-cap fibroatheroma (CaTCFA) – 0.

At 12 months, 2 ("thick"-cap) fibroatheromas showed transition to ("thick"-cap) calcified fibroatheromas. In ad-

dition, 1 ("thick"-cap) fibroatheroma evolved to a fibrocalcific lesion. Other plaques remained stable (low-risk) phenotype (absence of evolution), and no new lesions occurred. Full data for plaque phenotypes at baseline and at 12 months are presented, together with representative examples of the plaque (limited) evolution, in Figure 5.

Table I. Characteristics of the study group and medical therapy at discharge

Parameter	Value
Age [years]	59 (52–66)
Gender, woman	4 (18.20)
Diabetes	6 (27.3)
h/o smoking	3 (13.6)
Hypertension	8 (36.4)
Dyslipidaemia	20 (90.1)
Peak troponin I [ng/ml]	129.11 (85.88–180.3)
Peak CK-MB [U/l]	460 (345–767)
LVEF by cMRI (%)	38.5 (30–41)
LVEF by ECHO (%)	41 (33–43)
Stent diameter [mm]	3.0 (3.0–3.5)
Stent length [mm]	18 (18–26)
$CD34^+CXCR4^+$ cells, dose × 10^6	2.21 (1.63–2.54)
Medications at discharge:	
β-blocker	22 (100)
ACEI or ARB	21 (95.4)
Aldosterone antagonist	14 (63.6)
Statin	22 (100)
Aspirin	22 (100)
ADP receptor antagonist	22 (100)

Data are shown as number (proportion, %), or median (Q1–Q3). Total patient number is 22. LVEF – left ventricular ejection fraction, cMRI – cardiac magnetic resonance imaging, ECHO – echocardiography, ACEI – angiotensin-converting enzyme inhibitor, ARB – angiotensin receptor blocker, ADP – adenosine diphosphate; n – number. Troponin I upper limit normal is < 0.1ng/ml; CK-MB upper limit normal is < 24 U/l. See text for details.

Discussion

To monitor evolution of coronary artery atherosclerosis after using the intracoronary route for stem/progenitor cell delivery, this study used both conventional imaging of the arterial lumen and plaque (quantitative angiography, intravascular ultrasound) and a novel ultrasonographic image analysis algorithm that enables precise quantification of key functional components of the atherosclerotic plaque (quantitative virtual histology).

Our principal finding is absence of atherosclerosis progression in the infarct-related artery 12 months after using it as a route for perfusion administration of stem cells. Moreover, follow-up evaluation with the index techniques of visualization documented a moderate reduction in plaque burden and stenoses severity. The latter might result from maximized pharmacologic therapy in the study patients and/or it could be mediated by stem cell-dependent mechanisms.

Some initial studies labelled progression of IRA atherosclerosis after stem cell transcoronary administration as a stem cell-mediated mechanistic adverse effect [15, 16]. If confirmed, this would pose an important limitation in applicability of the transcoronary route for delivering cell-based therapies. This is important because the transcoronary route plays a fundamental role in administration of cell-based therapies to compromised myocardium. In particular, as demonstrated by labelled cell myocardial uptake studies [11, 12, 33], this route is mostly effective (with its efficacy degree related to the delivery

Table II. Characteristics of angiographic luminal stenoses in the IRA

Parameter	B/L	12-month F/U	*P*-value
MLD [mm]	1.43 (1.32–1.78)	1.7 (1.36–1.94)	0.349
DS (%)	29.5 (25.5–35.5)	26.5 (21–31.5)	0.012
RD [mm]	2.11 (1.85–2.55)	2.2 (1.89–2.6)	0.525

Data are shown as median (Q1–Q3), total n = 28. MLD – minimal lumen diameter, DS – diameter stenosis, RD – reference diameter, F/U – follow-up. See text for details.

Table III. Gray-scale IVUS characteristics of the study lesions

Parameter	Baseline	12-month follow-up	*P*-value
MLA [mm^2]	3.19 (2.46–3.92)	3.22 (2.59–3.94)	0.135
Peak PB (%)	66.27 (60.22–69.36)	64.56 (59.93–67.85)	0.009
AS (%)	33.75 (27.5–39.5)	31 (24.15–38)	0.004
MLD [mm]	1.69 (1.52–1.92)	1.73 (1.53–1.96)	0.724
DR-LA [mm^2]	4.58 (3.7–5.19)	4.52 (3.75–5)	0.371
DR-D [mm]	2.4 (2.18–2.53)	2.4 (2.1–2.55)	0.449
PR- LA [mm^2]	5.37 (4.38–6.07)	5.26 (4.39–6)	0.086
PR-D [mm]	2.61 (2.36–2.78)	2.57 (2.37–2.77)	0.119

Data are shown as median (Q1–Q3). Total number of IVUS-detected IRA lesions was 32. IVUS – intravascular ultrasound, MLA – minimal lumen area, PB – plaque burden, AS – area stenosis, DR-LA – distal reference lumen area, PR-LA – proximal reference lumen area, DR-LA – distal reference lumen area, DR-D – distal reference diameter, PR-D – proximal reference diameter. Area stenosis was calculated as 100 – MLA × 100/(0.5 × (DR-LA + PR-LA)).

techniques and cell types). Easiness to use and a good safety-and-feasibility to efficacy balance are important clinical advantages.

Vanderheyden *et al.* [15] and Mansour *et al.* [16] suggested that CD133+ (endothelial progenitor)–enriched bone marrow stem cells might stimulate in-stent neointimal proliferation and progression of distal-to-stent atherosclerosis. Such a potential effect, understood as a "tradeoff" inherent to therapies designed to enhance cardiac repair [16, 34], raised concerns with regard to using the transcoronary route for progenitor/stem cell delivery in further clinical trials. Some bench and animal model data seemed to support the "tradeoff" concept. For instance, a study of hindlimb ischemia in apolipoprotein E-knockout mice by Silvestre *et al.* [35] reported that transplantation of 1×10^6 bone marrow-derived mononuclear cells from wild-type animals accelerated atherosclerosis by inducing a significant (by ≈ 50–70%) increase in atherosclerotic lesion size in absence of an effect on plaque composition. At least one other study in the apolipoprotein E-knockout murine model suggested that transfer of bone marrow cells and endothelial progenitor cells may result in promotion of atherosclerosis [36]. George *et al.* [36] associated bone marrow and endotheli-

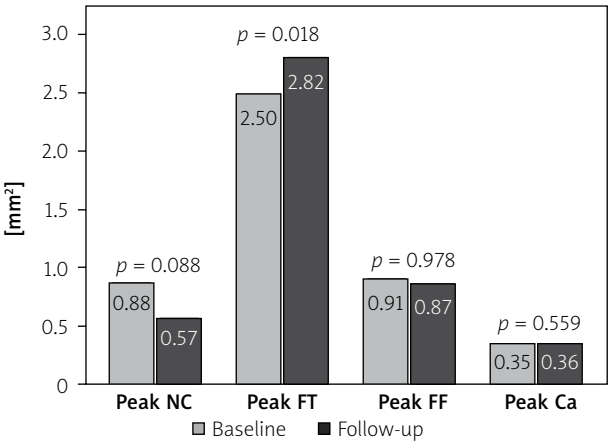

Figure 4. Evolution of the key components of atherosclerotic plaques by VH-IVUS. Bars show median values (baseline data in gray, 12-month follow-up data in black). Note a trend to reduction of peak necrotic core component (p = 0.088) and a mild increase in the fibrotic component, consistent with plaque stabilization

NC – necrotic core, FT – fibrotic, FF – fibro-fatty, Ca – dense calcium.

Table IV. VH-IVUS characteristics of the study lesions

Variable	Baseline	12-month F/U	*P*-value
Peak total content per plaque CSA[a]:			
Peak NC (%)	23.5 (16.18–34.37)	23.45 (12.26–29.05)	0.151
NC MLA [mm²]	0.37 (0.23–0.82)	0.36 (0.11–0.68)	0.487
NC MLA (%)	13.79 (8.27–22.01)	13.33 (4.57–21.5)	0.305
Peak FT (%)	70.41 (65.2–75.41)	75 (68.67–79.79)	0.004
FT MLA [mm²]	1.9 (1.35–2.48)	1.89 (1.47–2.81)	0.230
FT MLA (%)	56.15 (49.15–67.74)	64.88 (55.83–70.66)	0.009
Peak FF (%)	24.75 (15.65–41.1)	23 (16.48–31.48)	0.708
FF MLA [mm²]	0.51 (0.29–0.86)	0.51 (0.24–1.07)	0.805
FF MLA (%)	17.24 (7.9–25.24)	15.25 (9.13–31.1)	0.562
Peak Ca (%)	12.93 (7.94–19.8)	14.7 (7.17–23.4)	0.797
Ca MLA [mm²]	0.13 (0.02–0.31)	0.15 (0.05–0.4)	0.509
Ca MLA (%)	3.7 (0.58–11.33)	3.91 (1.76–14.1)	0.207
Peak total FF + NC [mm²]	1.75 (1.08–2.37)	1.55 (0.94–2.43)	0.786
Peak total FF + NC (%)	43 (36.7–49.11)	38.93 (36.1–46.71)	0.331
Confluent content[b]:			
confl. NC area [mm²]	0.64 (0.2–0.74)	0.59 (0.31–0.73)	0.290
confl. NC area per plaque CSA (%)	12.52 (6.45–20.95)	11.55 (7.45–19.15)	0.695
confl. NC arc [°]	64.55 (34–88.55)	58.1 (44.2–83.49)	0.937
confl. NC thickness [mm]	0.42 (0.28–0.46)	0.39 (0.32–0.48)	0.875
confl. Ca area [mm²]	0.36 (0.23–0.59)	0.41 (0.25–0.69)	0.155
confl. Ca arc [°]	53.4 (44.1–71.3)	61.9 (40.6–73.5)	0.991
Minimum FC thickness [mm][c]	0.15 (0.13–0.19)	0.16 (0.13–0.2)	0.646

Data are shown as median (Q1–Q3); n = 32. VH – virtual histology, CSA – cross-sectional plaque area (CSA = EEM area – lumen area, EEM – external elastic membrane), MLA – minimal lumen area, NC – necrotic core, FT – fibrotic component, FF – fibro-fatty component, Ca – dense calcium component, confl. – confluent. 'MLA' indicates measurements performed at the minimal lumen area spot. [a]Conventional VH-IVUS parameters ("automatic", provided by the routine VH software, expressed as a peak total content per plaque). [b]Peak confluent content per plaque (determined using qVH algorithm [21]). [c]To be considered measurable, the minimum fibrous cap (FC) thickness had to exceed the axial resolution of a 20 MHz IVUS transducer (120 µm).

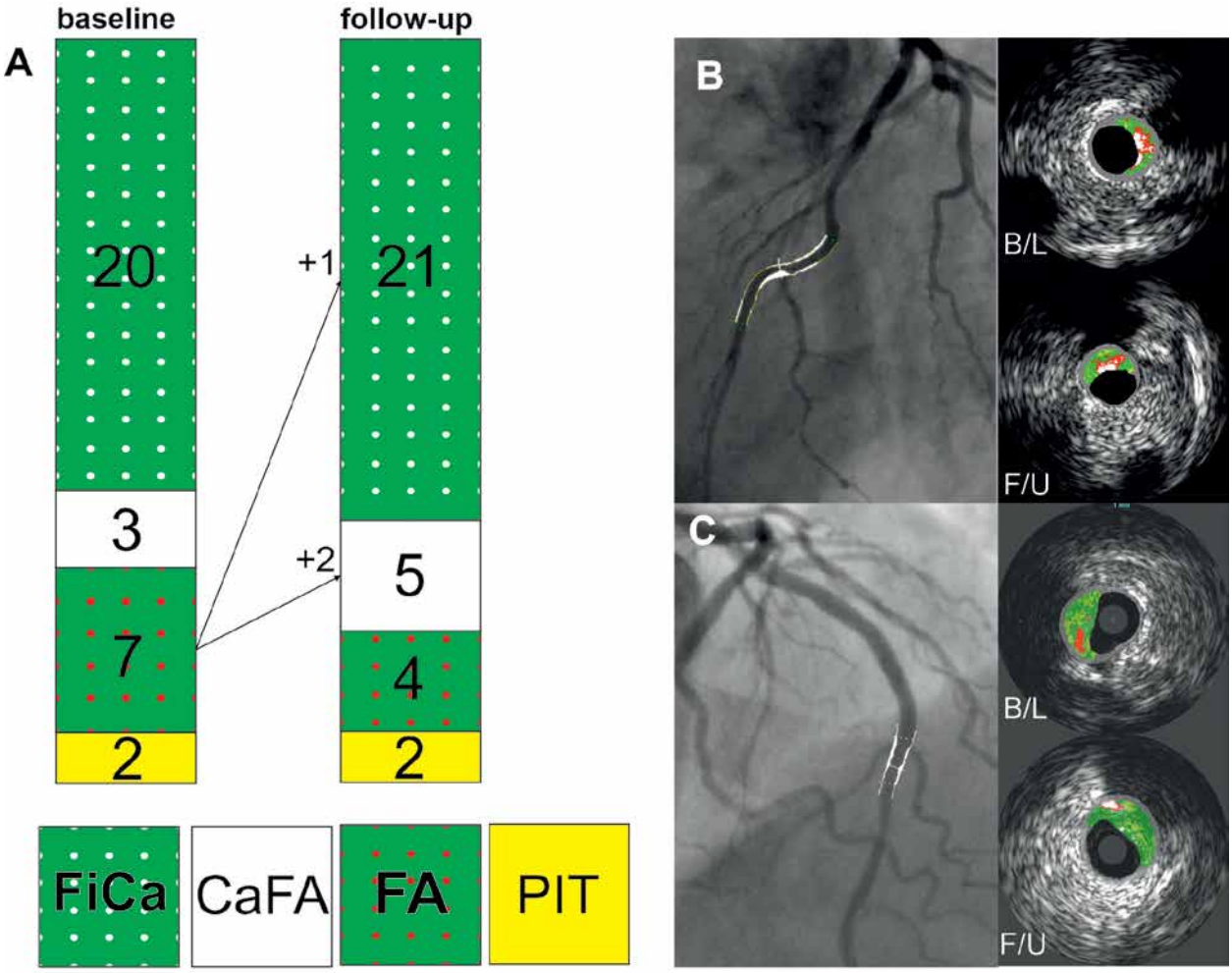

Figure 5. Evolution of infarct-related artery atherosclerotic plaque phenotypes in this study (A) and typical examples (B, C). Note that the overall plaque phenotype remained stable – both taken as an absence of "unstable" plaque phenotypes (thin-cap fibroatheroma, calcified thin-cap fibroatheroma) and (also) as a lack of any major changes in the individual plaque phenotypes (**A**). Two fibroatheromas (ie., "thick"-cap fibroatheroma) progressed to the calcified fibroatheroma phenotype and one other to the fibro-calcific phenotype (both phenotype changes consistent with an increase in plaque stability); the remaining 30 plaques maintained their phenotype (**A**). **B** is an example of a stable calcified fibroatheroma; **C** shows an evolution from a ("thick"-cap) fibroatheroma to a fibro-calcific plaque. Also note the importance of the use of landmarks to ensure that evaluation occurs at the same "site" at baseline and at 12 months

FiCa – fibrocalcific, CaFA – calcified fibroatheroma, FA – fibroatheroma ("thick-cap" fibroatheroma), PIT – pathological intimal thickening.

al progenitor cells with an increase in the atherosclerotic lesion size (via increasing lipid cores) whereas endothelial progenitor cells were also claimed to enhance thinning of the fibrous cap and thus reduce plaque stability [36].

Although bone marrow cells can differentiate into vascular cells that participate in the pathogenesis of atherosclerosis [37], other progenitor cell types – such as Wharton Jelly mesenchymal stem cells (umbilical cord stem cells) – have been found to stimulate neovascularization (and thus improve oxygen supply to the ischaemic tissue) in absence of any detectable stimulation of atherosclerosis progression [38]. These different (and seemingly contradictory) findings suggest that a "pro-" vs. "anti-" atherosclerotic (or neutral) effect of stem/progenitor cells may depend not only on the cell type but also, to some extent, on the study model, making detailed human studies (like ours) particularly relevant. Several recent reports indicate that mesenchymal stem cell transplantation may alleviate atherosclerosis by promoting an anti-inflammatory environment and inhibiting the atherosclerotic pathways [39, 40].

$CD34^{+}CXCR4^{+}$ stem/progenitor cells are spontaneously mobilized in AMI [41], and the magnitude of mobilization shows a positive correlation with improvement

in myocardial contractility at 12 months [41]. This is in agreement with the finding that higher counts of circulating progenitor cells, including $CD34^+CXCR4^+$ cells, are associated with better vascular function in the presence of risk factors [42]. In a recent study in 1366 subjects enrolled into the Emory Cardiovascular Biobank, lower counts (≤ median) of $CD34^+/CXCR4^+$ and $CD34^+/VEGFR2^+$ cells independently predicted all-cause mortality (HR = 1.46, 95% CI: 1.06–2.01, p = 0.02 and HR = 1.59, 95% CI: 1.15–2.18, p = 0.004) and cardiovascular death/myocardial infarction (HR = 1.50, 95% CI: 1.04–2.17, p = 0.03 and HR = 1.47, 95% CI: 1.01–2.03, p = 0.04) over a period of 3 years, compared to the individuals with lineages above the median value [43]. These findings are consistent with the anti-atherosclerotic and plaque-stabilizing effect of $CD34^+CXCR4^+$ cells suggested by our present findings (Figures 4, 5, Tables II–IV).

Recent work by the teams of Assmus *et al*. [9] and Qiu *et al*. [44] provides some evidence against any relevant pro-athrosclerotic effect of transcoronary-administered stem/progenitor cells in patients with AMI. Retrospective QCA measurements of the infarct target vessel in 83 patients with AMI treated with stent-assisted PCI (a control group) and in 83 patients receiving additional intracoronary progenitor cell infusion at 5 days post pPCI, with coronary angiography repeated at 4 months, showed that the late loss as a measure of neointima formation was similar between the control and the cell-treated group at follow-up (0.9 ±0.8 vs. 0.9 ±0.7 mm, p = 0.9) [9]. Stent restenosis rate was also comparable in both groups (35% control vs. 27% cell-treated group, p = 0.2), consistent with lack of any stimulatory effect of stem/progenitor cells on in-stent proliferation. The latter would have been, in any case, highly unlikely as the cells are typically administered distal to the stent. Unfortunately, any detailed assessment of atherosclerosis distal to the IRA stent was lacking [9]. Rather, these investigators based their conclusion only on a relatively low (28.9%) target vessel revascularization rate during a median of > 3 years of follow-up [9]. More detailed work by Qiu *et al*. [44] compared baseline and 4-month follow-up angiograms and IVUS images from STEMI patients treated with $CD133^+$ stem cell intracoronary injection after pPCI (n = 17) versus those obtained in patients who received placebo (n = 20). IRA analysis revealed similar changes in distal nonstented segment plaque burden between the stem cell and placebo groups (B/L – 41.9 vs. 37.4%, p = 0.56; F/U – 46.7 vs. 40.9%, p = 0.17) [44]. Findings also were similar for the distal non-culprit segment in patients receiving vs. not receiving stem cells [44]. Furthermore, in the contralateral coronary artery, there were no differences in changes in MLA, plaque burden, or attenuated plaque between stem cell and placebo patients [44]. The authors concluded that intracoronary injection of $CD133^+$ bone marrow stem cells had no IVUS-detectable effect on neointimal hyperplasia or atherosclerosis progression in either IRA or contralateral arteries [44]. In aggregate, these studies [9, 44] taken together with our present results (Tables II–IV) refute early data by Vanderheyden *et al.* [15] and Mansour *et al.* [16]. Moreover, our findings indicate regression of IRA atherosclerosis (Table II–IV) in patients subjected to delivery of progenitor/stem cells via the IRA.

Intravascular imaging plays a fundamental role in longitudinal studies of atherosclerosis evolution [45–50], including evaluation of plaque morphology (and its changes) in relation to atherosclerosis-mediated cardiac adverse clinical events such as MI and cardiac death [48, 51–54]. Intracoronary imaging is particularly important for its increased accuracy (against traditional planar analysis of intraarterial angiography images) of lesion detection and evaluation of its severity and morphology. Indeed, 87.5% of IVUS-identified lesions in this study could be detected with QCA (see Table III vs. Table II). Importantly, our study applied not only a range of routinely available state-of-the-art techniques (such as conventional IVUS, "automatic" VH image analysis limited to quantification of the "total" per plaque cross-sectional area NC/FF/FT/Ca and prone to several fundamental analysis artefacts [29, 30, 55] and other constraints [56]) but also a novel algorithm of qVH evaluation [21]. Recently validated qVH algorithm [21], with its precise evaluation of fundamental plaque biophysics-based characteristics [23, 24] (Figure 1), has been presently introduced for the first time in a longitudinal clinical study use (Figures 2, 3, Table IV). Because of significant limitations of conventional VH-IVUS image quantification revealed in prior studies, qVH appears to have several fundamental advantages [21] that may improve IVUS-based longitudinal research of coronary atherosclerosis.

Recent analysis by the Mayo Clinic group applied conventional VH-IVUS to evaluate plaque evolution in a series of 80 heart transplant receipients [57]. The study, using "automatic" (total content per plaque area) quantification of the necrotic core found that patients with greater yearly median change in necrotic core had lower levels of both $CD34^+CD133^+$ circulating progenitor cells (225 (130–518) vs. 470 (285–760) per 100 000 counts, p = 0.006) as well as $CD34^+$ cells (860 (485–2223) vs. 1840 (910–2590) per 100 000 counts, p = 0.05) [54]. Also, patients with TCFA at baseline IVUS examination had significantly lower levels of circulating $CD34^+$ $CD133^+$ cells (p = 0.03) [54]. These findings are consistent with a reduced progression of cardiac allograft vasculopathy and a reduction in cardiovascular events in relation to higher levels of circulating $CD34^+CD133^+$ progenitor cells [54].

Both IVUS-detected TCFA and TCFA by optical coherence tomography (OCT) is typically located proximal to the maximal lumen stenosis (minimal lumen area site), consistent with a "fire-and-smoke" mechanism [22]. The "fire-and-smoke" mechanism, initially identified for its pivotal role in pathology of acute coronary syndromes [58,

59] is also relevant as a basis for an increased risk of major adverse cardiac events in clinically stable patients with TCFA [53]. Although VH-IVUS detection of the atherosclerotic plaque 4 fundamental components has been validated against ex-vivo histology [60–62], the discriminatory power of conventional VH-IVUS findings (particularly in relation to future cardiac events) may be limited by use of a "total" (pixel-colour-generated) proportional content of FF/FT/NC/DC. This is now changed with plaque biophysics-based qVH evaluation (Figures 1, 3, Table IV) that we recently validated [21]. Further limitations of the conventional VH-IVUS analyses arise from inability to quantitatively discriminate artefacts [29, 30], use of different TCFA definitions use across studies [22, 48, 56, 63] as well as the "requirement" of the TCFA phenotype "presence" in 3 consecutive VH-IVUS frames" to determine the lesion as TCFA [23]. Because the radiofrequency image capture is triggered by the R have on ECG [22], the latter results in the dependence of TCFA identification on heart rate at the time of IVUS interrogation which is clearly flawed [55]. These limitations of conventional analysis lead to fragility of TCFA identification in over 40% coronary plaques getting labelled as a "TCFA" [56]. Those, very significant, considerations, indicate an important role for the recently validated qVH algorithm [21] that exhibits a very high reproducibility and minimal inter-observer and inter-transducer variability [21]. These features, suboptimal with conventional VH-IVUS image analysis algorithms [64] are critical in longitudinal studies of atherosclerosis.

One important advantage of IVUS, a sound-based modality, is its tissue penetration of ≈10 mm for a 20 MHz transducer [65]. This enables, in most cases, visualization of the entire coronary atherosclerotic plaque thickness that is critical for determining architecture of its key components [24, 25, 65] (cf., Figure 3) and for predicting plaque behaviour including the risk of rupture [24, 25, 66]. Axial resolution of 20M Hz IVUS catheters (such as the ones used in this study) is ≈120 µm and lateral resolution is ≈ 200 µm [65]. OCT is a light-based imaging modality whose resolution (12–15 µm axial, 20–40 µm lateral) is superior to that of IVUS [65]. This, however, occurs at the cost of very limited tissue penetration (≈1.0–2.5 mm) that enables to capture with OCT only the para-luminal segment of the atherosclerotic plaque [65]. Apart from the OCT inability to fully quantify critical constituents of the plaque (Figure 1), OCT is prone to image artefacts that may result (with histology as the benchmark) in misclassification of intimal thickening as fibroatheroma or thin cap fibroatheroma [67]. Adding VH-IVUS to OCT significantly reduced the error rate, indicating an important role for combined ("hybrid") IVUS-OCT imaging, taking advantage of the much greater tissue penetration with IVUS [65, 66]. However, it needs to be recognized that plaque progression and rupture are not solely determined by plaque configuration but also by mechanical factors [24, 25] that may induce instability and by active inflammation [21, 66].

One fundamental limitation of this study is the sample size that, by some, may be considered moderate. Another is lack of cohort not receiving cell administration. While absence of a control group of IRA-imaged patients not subjected to stem cell administration does not significantly affect conclusions from this study with regard to absence of atherosclerosis progression in association with transcoronary stem cell administration, it affects any insights into the mechanism(s) of atherosclerosis regression that we have observed in cell-treated arteries. In particular, regression of atherosclerosis may occur in relation to intensive medical therapy [45–47]. We received no approval to repeat invasive imaging in in the control group patients. Other limitations include our lack of evaluation of non-IRA arteries. However, any stem cell-mediated effects on non-IRA coronary arteries are not only unlikely with trans-IRA cell delivery [44], and those would be expected to occur similarly in arteries other than the coronaries. Axial resolution of IVUS (≈120 µm in 20-MHz transducers) is rather poor in relation to OCT [65]. Thus IVUS is unable to measure precisely the thickness of coronary artery rupture-prone fibrous cap whose histologic thickness is determined at ≈65 µm [27]. Of note, this is not a limitation in the carotid arteries where the fibrous cap critical for rupture risk is ≈200 µm [21]. Importantly, this (general) IVUS limitation is not directly applicable to data from this study because of absence of TCFA(s) amongst lesion phenotypes (Figure 5). As we identified a consistent (accross the imaging techniques) and statistically significant reduction in atherosclerosis over 12 months after transcoronary stem cell delivery, it is unlikely that a larger sample size would yield qualitatively different results. Nevertheless, it remains to be evaluated whether (and to what extent) the present findings are applicable to other stem cell types and doses.

Conclusions

This study, using both classic and novel imaging techniques including quantitative virtual histology, shows lack of any stimulatory effect of transcoronary stem cell transfer on coronary atherosclerosis. 12 months after transcoronary cell administration there was a reduction in stenosis severity by both angiography and intravascular ultrasound while virtual histology and quantitative virtual histology indicated stable – and further stabilizing – plaque phenotypes. This is reassuring for continued use of the transcoronary route for delivery of therapeutic cells to compromised myocardium. Further work is required to determine whether, and to what extent, the moderate reduction in plaque burden and atherosclerotic lumen reduction in mid-term after stem cell delivery results from optimized pharmacotherapy and/or transcoronary stem cell transfer.

Acknowledgments

Parts of this work were communicated to EuroPCR (W. Dabrowski MD, oral presentation abstract, 2020).

Supported by the Polish Ministry of Science and Higher Education and the National Centre for Science (PBZ-KBN-099/P05/2003, Myocardial Regeneration by Intracoronary Infusion of Selected Population of Stem Cells in Acute Myocardial Infarction, REGENT, and N402-184234, Carotid arteRy plaque morphology And atheroSclerosis biomarkers: Krakow Virtual Histology Study, CRACK-VH), Jagiellonian University Medical College (K/ZDS/005644; PM), Polish Cardiac Society/Servier Clinical Research in Atherosclerosis Grant and Polish Cardiac Society/ADAMED Grant for Basic Research in Atherosclerosis (to PM). Also supported by the John Paul II Hospital in Krakow Research Fund.

Conflict of interest

The authors declare no conflict of interest.

References

1. Bloemkolk D, Dimopoulou C, Forbes D, et al. Challenges and Opportunities for Cardiovascular Disease Research: Strategic Research Agenda for Cardiovascular Diseases (SRA-CVD) – a document for the European Commission. https://www.era-cvd.eu/media/content/ERA-CVD_SRA_05-2019-1.pdf (accessed 30 September 2022).
2. Timmis A, Vardas P, Townsend N, et al. European Society of Cardiology: cardiovascular disease statistics 2021. Eur Heart J 2022; 43: 716-99.
3. Pearson J, Sipido KR, Musialek P, van Gilst WH. The Cardiovascular Research community calls for action to address the growing burden of cardiovascular disease. Cardiovasc Res 2019; 115: e96-8.
4. Bolli R, Solankhi M, Tang XL, Kahlon A. Cell therapy in patients with heart failure: a comprehensive review and emerging concepts. Cardiovasc Res 2022; 118: 951-76.
5. Braunwald E. Cell-based therapy in cardiac regeneration: an overview. Circ Res 2018; 123: 132-7.
6. Menasché P. Cell therapy trials for heart regeneration – lessons learned and future directions. Nat Rev Cardiol 2018; 15: 659-71.
7. Drabik L, Mazurek A, Dzieciuch-Rojek M, et al. Trans-endocardial delivery of progenitor cells to compromised myocardium using the "needle technique" and risk of myocardial injury. Adv Interv Cardiol 2022; 18: 423-30.
8. Tendera M, Wojakowski W, Ruzyłło W, et al. Intracoronary infusion of bone marrow-derived selected $CD34^+CXCR4^+$ cells and non-selected mononuclear cells in patients with acute STEMI and reduced left ventricular ejection fraction: results of randomized, multicentre Myocardial Regeneration by Intracoronary Infusion of Selected Population of Stem Cells in Acute Myocardial Infarction (REGENT) Trial. Eur Heart J 2009; 30: 1313-21.
9. Assmus B, Walter DH, Lehmann R, et al. Intracoronary infusion of progenitor cells is not associated with aggravated restenosis development or atherosclerotic disease progression in patients with acute myocardial infarction. Eur Heart J 2006; 27: 2989-95.
10. Kooreman NG, Ransohoff JD 1, Wu JC. Tracking gene and cell fate for therapeutic gain. Nature Materials 2014; 13: 106-9.
11. Musialek P, Tekieli L, Kostkiewicz M, et al. Randomized transcoronary delivery of $CD34^+$ cells with perfusion versus stop-flow method in patients with recent myocardial infarction: early cardiac retention of ^{99m}Tc-labeled cells activity. J Nucl Cardiol 2011; 18: 104-16.
12. Musialek P, Tekieli L, Kostkiewicz M, et al. Infarct size determines myocardial uptake of $CD34^+$ cells in the peri-infarct zone: results from a study of ^{99m}Tc-extametazime-labeled cell visualization integrated with cardiac magnetic resonance infarct imaging. Circ Cardiovasc Imaging 2013; 6: 320-8.
13. Bilewska A, Abdullah M, Mishra R, et al. Safety and efficacy of intracoronary delivery of human neonatal stem cells using a novel system (CIRCULATE catheter) in swine model of acute myocardial infarction. Adv Interv Cardiol 2022; 18: 431-8.
14. Musialek P, Mazurek A, Jarocha D, et al. Myocardial regeneration strategy using Wharton's jelly mesenchymal stem cells as an off-the-shelf 'unlimited' therapeutic agent: results from the Acute Myocardial Infarction First-in-Man Study. Adv Interv Cardiol 2015; 11: 100-7.
15. Vanderheyden M, Mansour S, Bartunek J. Accelerated atherosclerosis following intracoronary haematopoietic stem cell administration. Heart 2005; 91: 448.
16. Mansour S, Vanderheyden M, De Bruyne B, et al. Intracoronary delivery of hematopoietic bone marrow stem cells and luminal loss of the infarct-related artery in patients with recent myocardial infarction. J Am Coll Cardiol 2006; 47: 1727-30.
17. Nishimura RA, Edwards WD, Warnes CA, et al. Intravascular ultrasound imaging: In vitro validation and pathologic correlation. J Am Coll Cardiol 1990; 16: 145-54.
18. Mintz GS, Nissen SE, Anderson WD, et al. American College of Cardiology Clinical Expert Consensus Document on Standards for Acquisition, Measurement and Reporting of Intravascular Ultrasound Studies (IVUS). A report of the American College of Cardiology. Task Force on Clinical Expert Consensus Documents. J Am Coll Cardiol 2001; 37: 1478-92.
19. Mintz GS. Imaging controls. In: Cardiovascular Ultrasound. Mintz GS (ed.). Taylor&Francis 2005; 14-5.
20. Maehara A, Cristea E, Mintz GS, et al. Definitions and methodology for the grayscale and radiofrequency intravascular ultrasound and coronary angiographic analyses. JACC Cardiovasc Imaging 2012; 5 (3 Suppl): S1-9.
21. Musialek P, Dabrowski W, Mazurek A, et al. Quantitative virtual histology for in vivo evaluation of human atherosclerosis – a plaque biomechanics-based novel image analysis algorithm: validation and applications to atherosclerosis research. In: Intravascular Ultrasound: From Acquisition to Advanced Quantitative Analysis. Balocco S (ed.). Elsevier 2020; 71-96.
22. König A, Margolis MP, Virmani R, et al. Technology insight: In vivo coronary plaque classification by intravascular ultrasonography radiofrequency analysis. Nat Clin Pract Cardiovasc Med 2008; 5: 219-29.
23. García-García HM, Mintz GS, Lerman A, et al. Tissue characterisation using intravascular radiofrequency data analysis: recommendations for acquisition, analysis, interpretation and reporting. EuroIntervention 2009; 5: 177-89.
24. Finet G, Ohayon J, Rioufol G. Biomechanical interaction between cap thickness, lipid core composition and blood pressure in vulnerable coronary plaque: impact on stability or instability. Coron Artery Dis 2004; 15: 13-20.
25. Ohayon J, Finet G, Gharib AM, et al. Necrotic core thickness and positive arterial remodeling index: emergent biomechanical factors for evaluating the risk of plaque rupture. Am J Physiol Heart Circ Physiol 2008; 295: H717-27.

26. Siewiorek GM, Loghmanpour NA, Winston BM, et al. Reproducibility of IVUS border detection for carotid atherosclerotic plaque assessment. Med Eng Phys 2012; 34: 702-8.
27. Narula J, Nakano M, Virmani R, et al. Histopathologic characteristics of atherosclerotic coronary disease and implications of the findings for the invasive and noninvasive detection of vulnerable plaques. J Am Coll Cardiol 2013; 61: 1041-51.
28. Kubo T, Maehara A, Mintz GS, et al. The dynamic nature of coronary artery lesion morphology assessed by serial virtual histology intravascular ultrasound tissue characterization. J Am Coll Cardiol 2010; 55: 1590-7.
29. Murray SW, Palmer ND. What is behind the calcium? The relationship between calcium and necrotic core on virtual histology analyses. Eur Heart J 2009; 30: 125.
30. Sales FJ, Falcão BA, Falcão JL, et al. Evaluation of plaque composition by intravascular ultrasound "virtual histology": the impact of dense calcium on the measurement of necrotic tissue. EuroIntervention 2010; 6: 394-9.
31. Zalewski J, Zmudka K, Musialek P, et al. Detection of microvascular injury by evaluating epicardial blood flow in early reperfusion following primary angioplasty. Int J Cardiol 2004; 96: 389-96.
32. Musiałek P. TASTE-less endpoint of 30-day mortality (and some other issues with TASTE) in evaluating the effectiveness of thrombus aspiration in STEMI: not the "evidence" to change the current practice of routine consideration of manual thrombus extraction. Pol Heart J 2014; 72: 479-87.
33. Tekieli L, Kwiecien E, Szot W, et al. Single-photon emission computed tomography as a fundamental tool in evaluation of myocardial reparation and regeneration therapies. Adv Interv Cardiol 2022; 18: 326-39.
34. Epstein ES, Stabile E, Kinnaird T, et al. Janus phenomenon: the interrelated tradeoffs inherent in therapies designed to enhance collateral formation and those designed to inhibit atherogenesis. Circulation 2004; 109: 2826-31.
35. Silvestre JS, Gojova A, Brun V, et al. Transplantation of bone marrow-derived mononuclear cells in ischemic apolipoprotein E-knockout mice accelerates atherosclerosis without altering plaque composition. Circulation 2003; 108: 2839-42.
36. George J, Afek A, Abashidze A, et al. Transfer of endothelial progenitor and bone marrow cells influences atherosclerotic plaque size and composition in apolipoprotein E knockout mice. Arterioscler Thromb Vasc Biol 2005; 25: 2636-41.
37. Sata M, Saiura A, Kunisato A, et al. Hematopoietic stem cells differentiate into vascular cells that participate in the pathogenesis of atherosclerosis. Nature Med 2002; 8: 403-9.
38. Musiał-Wysocka A, Kot M, Sułkowski M, Majka M. Regenerative potential of the product "CardioCell" derived from the Wharton's jelly mesenchymal stem cells for treating hindlimb ischemia. Int J Mol Sci 2019; 20: 4632.
39. Yao G, Qi J, Li X, et al. Mesenchymal stem cell transplantation alleviated atherosclerosis in systemic lupus erythematosus through reducing MDSCs. Stem Cell Res Ther 2022; 1: 328.
40. Kirwin T, Gomes A, Amin R, et al. Mechanisms underlying the therapeutic potential of mesenchymal stem cells in atherosclerosis. Regen Med 2021; 16: 669-82.
41. Wyderka R, Wojakowski W, Jadczyk T, et al. Mobilization of CD34+CXCR4+ stem/progenitor cells and the parameters of left ventricular function and remodeling in 1-year follow-up of patients with acute myocardial infarction. Mediators Inflamm 2012; 2012: 564027.
42. Moazzami K, Mehta A, Young A, et al. The association between baseline circulating progenitor cells and vascular function: the role of aging and risk factors. Vasc Med 2022; 27: 532-41.
43. Dhindsa DS, Desai SR, Jin Qi, et al. Circulating progenitor cells and outcomes in patients with coronary artery disease. Int J Cardiol 2023; 373: 7-16.
44. Qiu F, Maehara A, El Khoury R, et al. Impact of intracoronary injection of $CD133^+$ bone marrow stem cells on coronary atherosclerotic progression in patients with STEMI: a COMPARE-AMI IVUS substudy. Coron Artery Dis 2016; 27: 5-12.
45. Jensen LO, Thayssen P, Pedersen KE, et al. Regression of coronary atherosclerosis by simvastatin: a serial intravascular ultrasound study. Circulation 2004; 110: 265-70.
46. Waseda K, Ozaki Y, Takashima H, et al. Impact of angiotensin II receptor blockers on the progression and regression of coronary atherosclerosis: an intravascular ultrasound study. Circ J 2006; 70: 1111-5.
47. Hiro T, Kimura T, Morimoto T, et al. Effect of intensive statin therapy on regression of coronary atherosclerosis in patients with acute coronary syndrome: a multicenter randomized trial evaluated by volumetric intravascular ultrasound using pitavastatin versus atorvastatin (JAPAN-ACS [Japan assessment of pitavastatin and atorvastatin in acute coronary syndrome] study). J Am Coll Cardiol 2009; 54: 293-302.
48. Stone GW, Maehara A, Lansky AJ, et al. A prospective natural-history study of coronary atherosclerosis. N Engl J Med 2011; 364: 226-35.
49. Wykrzykowska JJ, Mintz GS, Garcia-Garcia HM, et al. Longitudinal distribution of plaque burden and necrotic core-rich plaques in nonculprit lesions of patients presenting with acute coronary syndromes. JACC Cardiovasc Imaging 2012; 5 (3 Suppl): S10-8.
50. Zheng B, Mintz GS, McPherson JA, et al. Predictors of plaque rupture within nonculprit fibroatheromas in patients with acute coronary syndromes: the PROSPECT study. JACC Cardiovasc Imaging 2015; 8: 1180-7.
51. Kedhi E, Berta B, Roleder T, et al. Thin-cap fibroatheroma predicts clinical events in diabetic patients with normal fractional flow reserve: the COMBINE OCT-FFR trial. Eur Heart J 2021; 42: 4671-9.
52. Fabris E, Berta B, Roleder T, et al. Thin-cap fibroatheroma rather than any lipid plaques increases the risk of cardiovascular events in diabetic patients: insights from the COMBINE OCT-FFR trial. Circ Cardiovasc Interv 2022; 15: e011728.
53. Roleder-Dylewska M, Gasior P, Hommels TM, et al. Morphological characteristics of lesions with thin cap fibroatheroma-a substudy from the COMBINE (OCT-FFR) trial. Eur Heart J Cardiovasc Imaging 2022; doi: 10.1093/ehjci/jeac218.
54. Fabris E, Berta B, Hommels T, et al. Long-term outcomes of patients with normal fractional flow reserve and thin-cap fibroatheroma. EuroIntervention 2023; 18: e1099-107.
55. Musialek P. Virtual histology intravascular ultrasound evaluation of atherosclerotic carotid artery stenosis: time for a fully quantitative image analysis. J Endovasc Ther 2013; 20: 589-94.
56. Obaid DR, Calvert PA, McNab D, et al. Identification of coronary plaque sub-types using virtual histology intravascular ultrasound is affected by inter-observer variability and differences in plaque definitions. Circ Cardiovasc Imaging 2012; 5: 86-93.
57. Ozcan I, Toya T, Corban MT, et al. Circulating progenitor cells are associated with plaque progression and long-term outcomes in heart transplant patients. Cardiovasc Res 2022; 118: 1703-12.

58. Legutko J, Jakala J, Mintz GS, et al. Virtual histology-intravascular ultrasound assessment of lesion coverage after angiographically-guided stent implantation in patients with ST elevation myocardial infarction undergoing primary percutaneous coronary intervention. Am J Cardiol 2012; 109: 1405-10.
59. Legutko J, Jakala J, Mintz G et al. Radiofrequency intravascular ultrasound assessment of lesion coverage after angiography-guided emergent percutaneous coronary intervention in patients with non-ST elevation myocardial infarction. Am J Cardiol 2013; 112: 1854-9.
60. Nair A, Kuban BD, Tuzcu EM, et al. Coronary plaque classification with intravascular ultrasound radiofrequency data analysis. Circulation 2002; 106: 2200-6.
61. Nair A, Margolis MP, Kuban BD, Vince DG. Automated coronary plaque characterisation with intravascular ultrasound backscatter: ex vivo validation. EuroIntervention 2007; 3: 113-20.
62. Muramatsu T, García-García HM, Brugaletta S, et al. Reproducibility of intravascular ultrasound radiofrequency data analysis (virtual histology) with a 45-MHz rotational imaging catheter in ex vivo human coronary arteries. J Cardiol 2015; 65: 134-42.
63. Calvert PA, Obaid DR, O'Sullivan M, et al. Association between IVUS findings and adverse outcomes in patients with coronary artery disease: the VIVA (VH-IVUS in Vulnerable Atherosclerosis) study. JACC Cardiovasc Imaging 2011; 4: 894-901.
64. Rodriguez-Granillo GA, Vaina S, García-García HM, et al. Reproducibility of intravascular ultrasound radiofrequency data analysis: implications for the design of longitudinal studies. Int J Cardiovasc Imaging 2006; 22: 621-31.
65. Regar E. Invasive imaging technologies: can we reconcile light and sound? J Cardiovasc Med 2011; 12: 562-70.
66. Costopoulos C, Brown AJ, Teng Z, et al. Intravascular ultrasound and optical coherence tomography imaging of coronary atherosclerosis. Int J Cardiovasc Imaging 2016; 321: 189-200.
67. Goderie TPM, van Soest G, Garcia-Garcia HM, et al. Combined optical coherence tomography and intravascular ultrasound radio frequency data analysis for plaque characterization. Classification accuracy of human coronary plaques in vitro. Int J Cardiovasc Imaging 2010; 26: 843-50.